SUPPLEMENTAL DATA

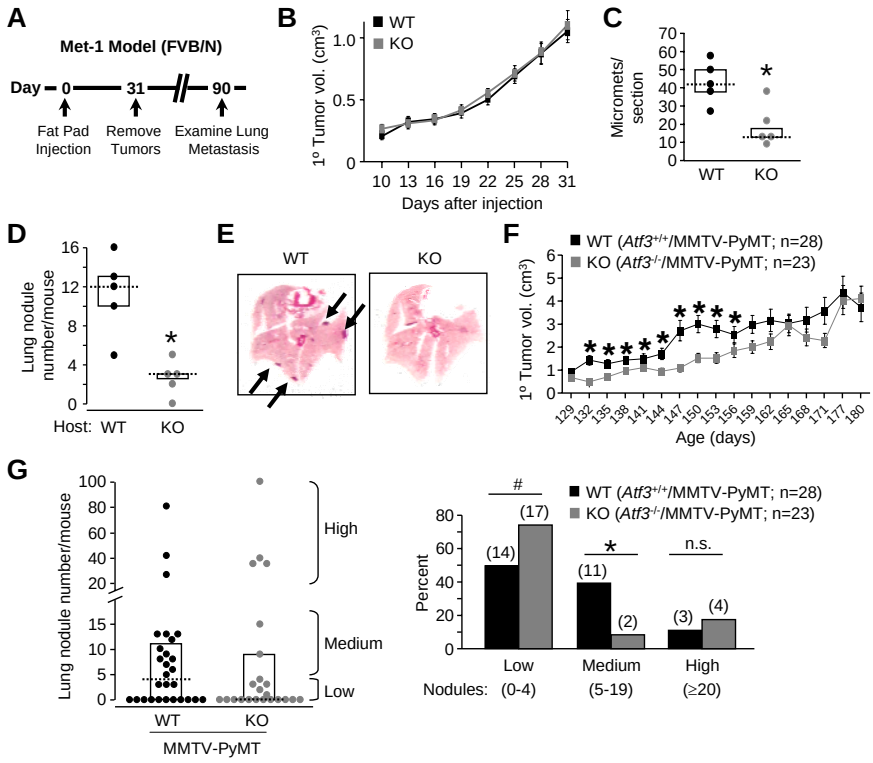

Figure S1

Atf3 deficiency reduces cancer development. **(A)** A schematic of the orthotopic model injecting turbo GFP (tGFP)-labeled Met-1 cells in FVB/N mice. **(B)** 1º tumors from WT (*Atf3*$^{+/+}$) or KO (*Atf3*$^{-/-}$) mice were measured by caliper and the volume (vol.) calculated (mean ± SEM, n = 5 mice per group, no statistical difference between groups). Mann-Whitney test was used for this panel and panels (C) and (D) below. **(C)** Lung micro-metastases (micromets) were counted at high magnification from sections stained for tGFP by immunohistochemistry (mean ± SEM, n = 5, **P* < 0.05). **(D)** WT or KO FVB/N mice were injected with Met-1 cells by tail vein and lung micromets were counted from H&E stained sections at 21 days after injection (n = 5 mice per group, **P* < 0.05). **(E)** Representative images of the lungs from (D) are shown. Arrows indicate some of the lung colonies. **(F)** 1º tumors from MMTV-PyMT transgenic mice in the WT or *Atf3* KO background were measured at the indicated age (X-axis) and the sum of tumor volumes from all fat pads that developed tumors was obtained for each mouse. The mean ± SEM of tumor volume for WT versus KO group was shown in Y-axis (**P* < 0.05, Student's t-test). **(G)** Lung metastasis of mice from panel (F) was analyzed at age 180 days. Left panel: Lung nodule numbers are shown in box-and-whisker plot. Mice showed heterogeneous phenotypes and can be clustered into three metastasis groups based on their nodule numbers: low (0-4), medium (5-19), and high (≥20). Right panel: Percentage of mice in each metastasis group is shown in Y-axis and numbers above the bars indicate the number of mice in the respective metastasis group (**P* < 0.02; # *P* ~0.08, Chi square analyses). n.s.: not significant.

A

Modulation by ATF3	Protein Name	Effect on Metastasis
Up-regulated	ANGPTL2	↑
	CCL2	↑
	CSF1	↑
	CXCL6	↑
	IL1a	↑
	MMP2	↑
	MMP9	↑
	MMP14	↑
	OPN (SPP1)	↑
	PLAU	↑
	CXCL12 (SDF1)	↑
	SHH	↑
	TGFB1	↑
	TGFB2	↑
	VEGFC	↑
	CXCL3	↑ *
	IL17	↓ or ↑
	TSP1	↓ or ↑
	LTA	↓
	TFPI	↓
	PTX3	↓ *
Down-regulated	FST	↓
	IL2	↓
	DKK1	↓ or ↑
	IL6	↓ or ↑
	FGF2	↑
	IL23	↑

B

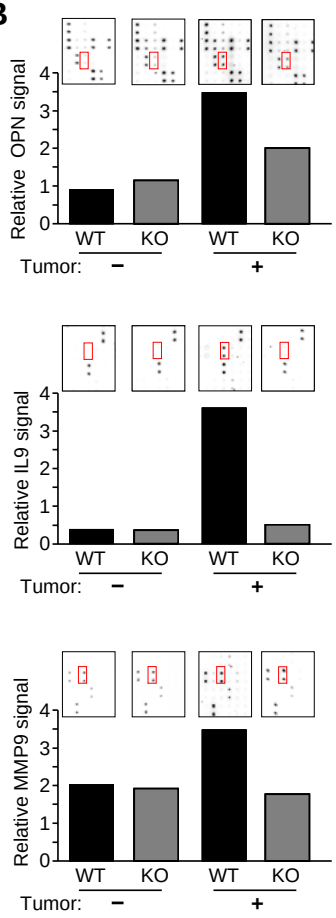

Figure S2

Plasmas from tumor-bearing WT and *Atf3* KO mice show different levels of soluble factors. **(A)** Plasmas from WT (*Atf3*$^{+/+}$) or KO (*Atf3*$^{-/-}$) C57BL/6 mice with or without PyMT tumors (n = 5 mice per group) were isolated at 30 days after cancer cell injection and analyzed by an antibody array that detected 308 proteins (RayBio®, L-series antibody array). After subtracting the background, the signals from WT mice without tumors were arbitrarily defined as 1. 107 candidates fit the following criteria: (a) soluble factors, (b) modulated (up- or down-regulated) by tumor development in the WT plasma (>1.3 fold difference), and (c) showing differential levels in the KO- versus WT-tumor bearing mice. Among these candidates, 27 have been documented to modulate or correlate with metastasis and are listed. Arrows indicate their roles in metastasis according to literature: up for enhancing and down for repressing; * indicates factors with data showing correlation but no data for causal relationship. Proteins with higher levels in the WT than KO plasma are classified as up-regulated (directly or indirectly) by ATF3, and vice versa. Most of these factors were up-regulated by ATF3 and are known to promote metastasis; only six were down-regulated by ATF3 and four of them are likely to repress metastasis. Thus, the direction of regulation by ATF3 for majority of the candidates is consistent with the finding that ATF3 in the host enhances metastasis. **(B)** Bar graphs for the indicated soluble proteins are shown, with insets showing the array blots. Red boxes indicate the duplicate spots of the respective proteins.

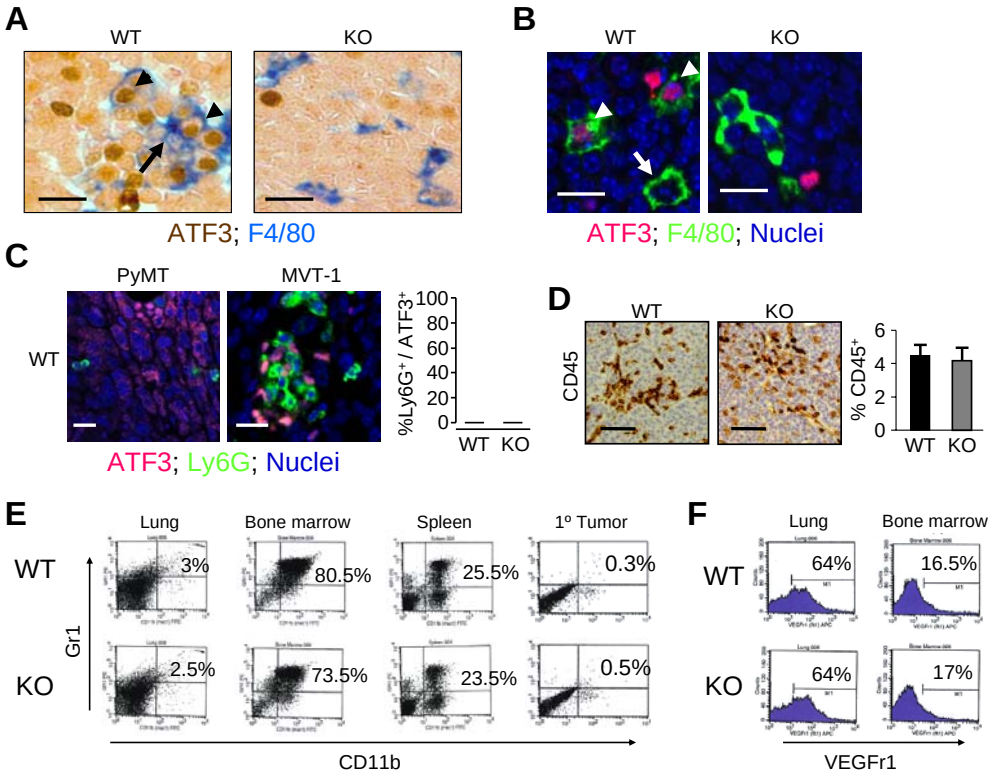

Figure S3

Analyses of various immune cells in tumors and other tissues. **(A)** WT (*Atf3*$^{+/+}$) or KO (*Atf3*$^{-/-}$) C57BL/6 mice were injected with PyMT cells and 1º tumors at 25 days after injection were analyzed by co-immunohistochemistry for ATF3 (brown) or F4/80 (blue). As shown, some macrophages in the WT host had *Atf3* expression (arrowhead), but some do not (arrow). The ATF3-positive cells in the KO panel are presumably the cancer cells since the PyMT cells are *Atf3*$^{+/+}$. Scale bars = 15µm. **(B)** WT (*Atf3*$^{+/+}$) or KO (*Atf3*$^{-/-}$) FVB/N mice were injected with MVT-1 cells and 1º tumors at 35 days after injection were analyzed by co-immunofluorescence for ATF3 (red) and F4/80 (green), with Topro-3 stain (blue) to indicate the nuclei. As shown, some macrophages in the WT host had *Atf3* expression (arrowhead), but some do not (arrow). The ATF3-positive cell in the KO panel is presumably the MVT-1 cancer cell. Scale bars = 15µm. **(C)** Same as (B) except that tumors from WT host injected with either PyMT or MVT-1 cells were analyzed: ATF3 (red), Ly6G (green, a neutrophil marker), Topro-3 (blue). Scale bars = 15µm. **(D)** Same as (A), except 1º tumors were analyzed for CD45, a general marker for hematopoietic cells, by immunohistochemistry (left panel; counterstained with hematoxylin) or by flow cytometry (right panel). Flow cytometry data represent the mean ± SEM (n = 5, no statistical difference between groups, Mann-Whitney test). Scale bars = 100µm. **(E)** Same as (A), except the indicated tissues were analyzed by flow cytometry for CD11b and Gr-1 double-positive cells. A representative dot plot from three mice is shown for lung, bone marrow, spleen, and 1º tumor (no statistical differences between groups, Mann-Whitney test). **(F)** Same as (A), except the indicated tissues were analyzed by flow cytometry for VEGFr1. A representative histogram from three mice is shown (no statistical differences between groups, Mann-Whitney test).

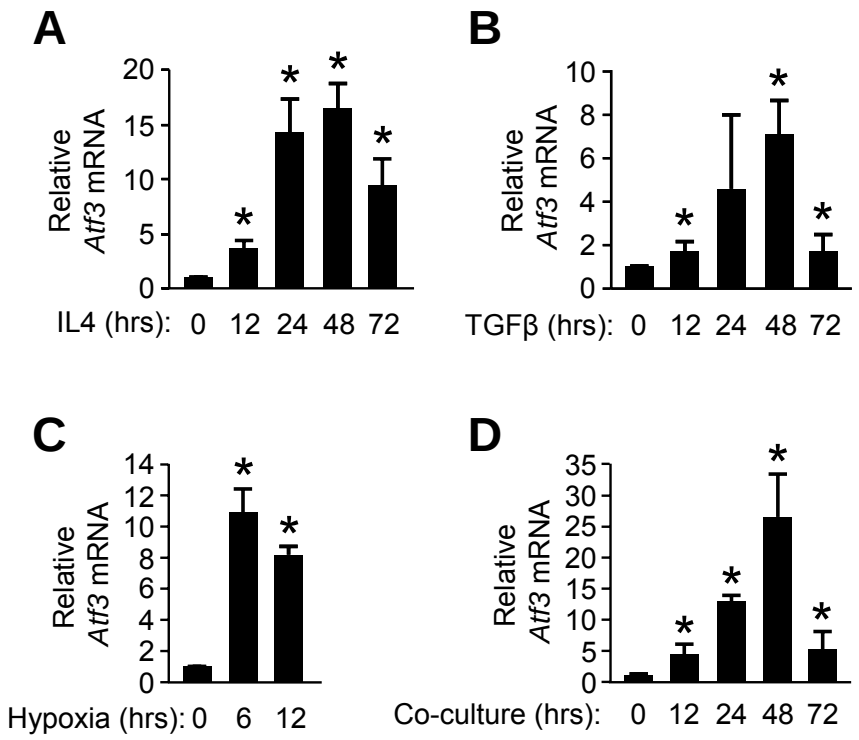

Figure S4

Induction of *Atf3* in bone marrow-derived macrophages by signals relevant to tumor microenvironment. **(A-B)** Bone marrow-derived macrophages ($Atf3^{+/+}$) were treated with IL4 or TGFβ (both of which have been shown to skew macrophages to the pro-cancer M2 pattern; 1) for the indicated time (hrs) and analyzed by RT-qPCR for *Atf3* mRNA. The signals were standardized against tubulin and the standardized signals at time point 0 were arbitrarily defined as 1. **(C)** Same as (A), except the cells were treated by hypoxia (1% O_2), a condition in the tumor microenvironment known to facilitate metastasis (a review, 2). **(D)** Bone marrow-derived macrophages were co-cultured with the PyMT cancer epithelial cells in Boyden chamber for the indicated time and analyzed by RT-qPCR as in (A). For all panels, a representative result from three to four independent experiments is show (mean ± SEM from triplicates, $*P < 0.05$ versus time point 0, Students t-test).

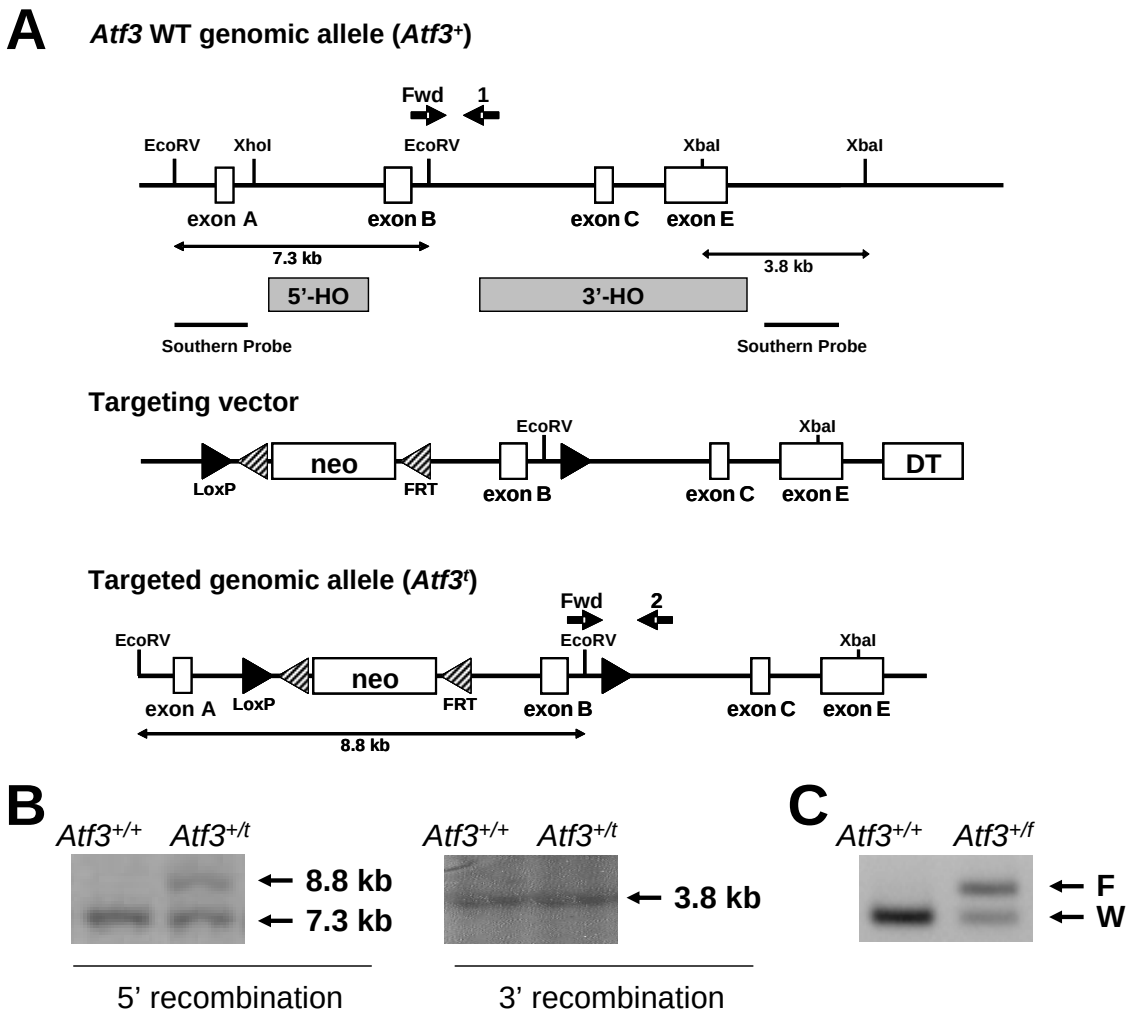

Figure S5

Analyses of WT and genetically modified *Atf3* alleles. **(A)** Schematics of the *Atf3* genomic allele (*Atf3*$^{+}$), the targeting vector, and the targeted allele upon homologous recombination (*Atf3*^{t}) are shown. Indicated are 5'- and 3'-homologous (HO) regions, restriction enzymes and probes for Southern blot. **(B)** Genomic DNAs from 129sv ES cells carrying the WT (*Atf3*$^{+}$) and *Atf3*^{t} alleles were analyzed by Southern blot for 5' (left panel) or 3' (right panel) recombination using the restriction enzymes and probes indicated in panel (A). Arrows on the right indicate the WT and *Atf3*^{t} alleles. **(C)** Genomic DNAs from mice carrying the WT and *Atf3* flox allele with the neo cassette deleted (*Atf3*^{f}) were analyzed by PCR genotyping using the primers indicated in (A) as forward (Fwd), Reverse #1 (1), and Reverse #2 (2). Arrows on the right indicate the bands for WT (W) and *Atf3*^{f} (F) alleles.

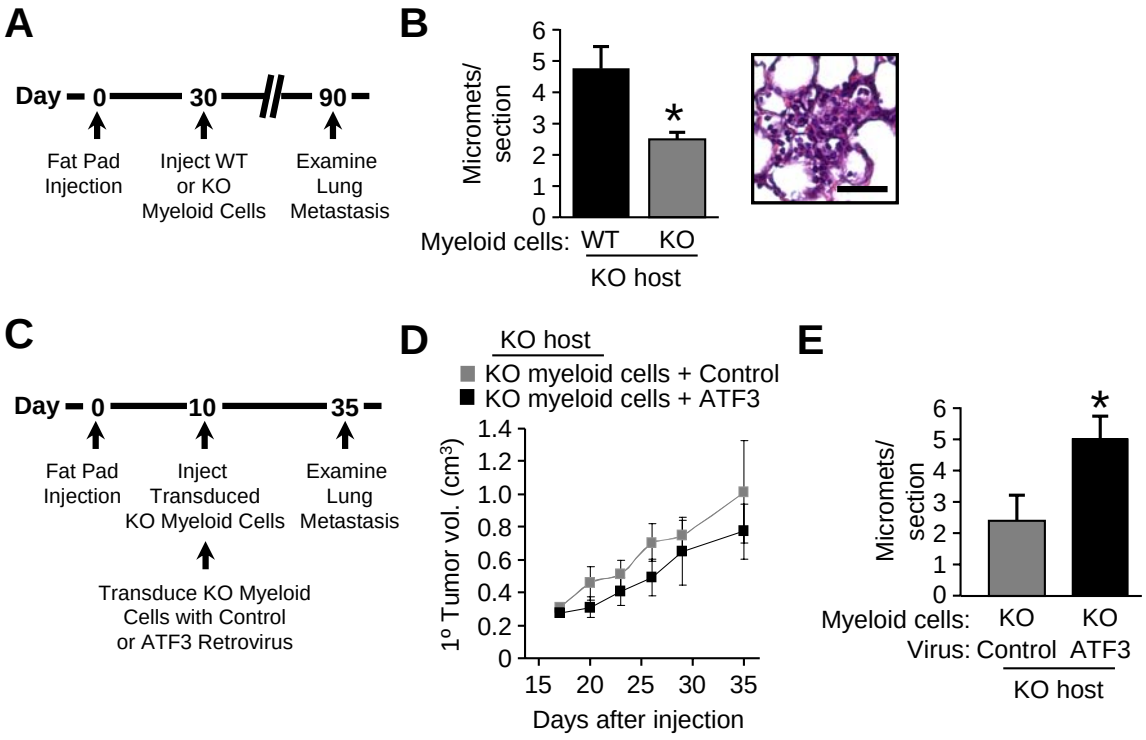

Figure S6

The effect of CD11b^{+} cells on cancer metastasis in *Atf3* KO mice. **(A)** A schematic of the sequential injection experiment: inject *Atf3* KO (*Atf3*$^{-/-}$) C57BL/6 mice with PyMT cancer cells in the mammary fat pad (day 0), followed by tail vein injection of WT (*Atf3*$^{+/+}$) or KO (*Atf3*$^{-/-}$) CD11b^{+} cells (day 30), and analysis of lungs (day 90). **(B)** Left: Micrometastases (micromets) were counted from H&E stained sections at high magnification (mean ± SEM, n = 5 mice per group, **P* < 0.05); right: a representative micromet image is shown. Scale bar = 50μm. Mann-Whitney test was used in this panel and panels (D) and (E) below. **(C)** A schematic of the add-back experiment using the sequential injection design: inject *Atf3* KO (*Atf3*$^{-/-}$) FVB/N mice with MVT-1 cancer cells in the mammary fat pad (day 0), followed by tail vein injection of *Atf3* KO CD11b^{+} cells with or without ATF3-add back (day 10), and analysis of lungs (day 35). Add-back was achieved using retrovirus expressing ATF3 under the CD68 mini-gene cassette (CD68-ATF3-IRES-Venus) or vector only (CD68-IRES-Venus). **(D)** 1º tumors from (C) were measured (mean ± SEM, n = 5 mice per group, no statistical difference between groups). **(E)** Micromets from (C) were counted using H&E stained sections (mean ± SEM, **P* < 0.05).

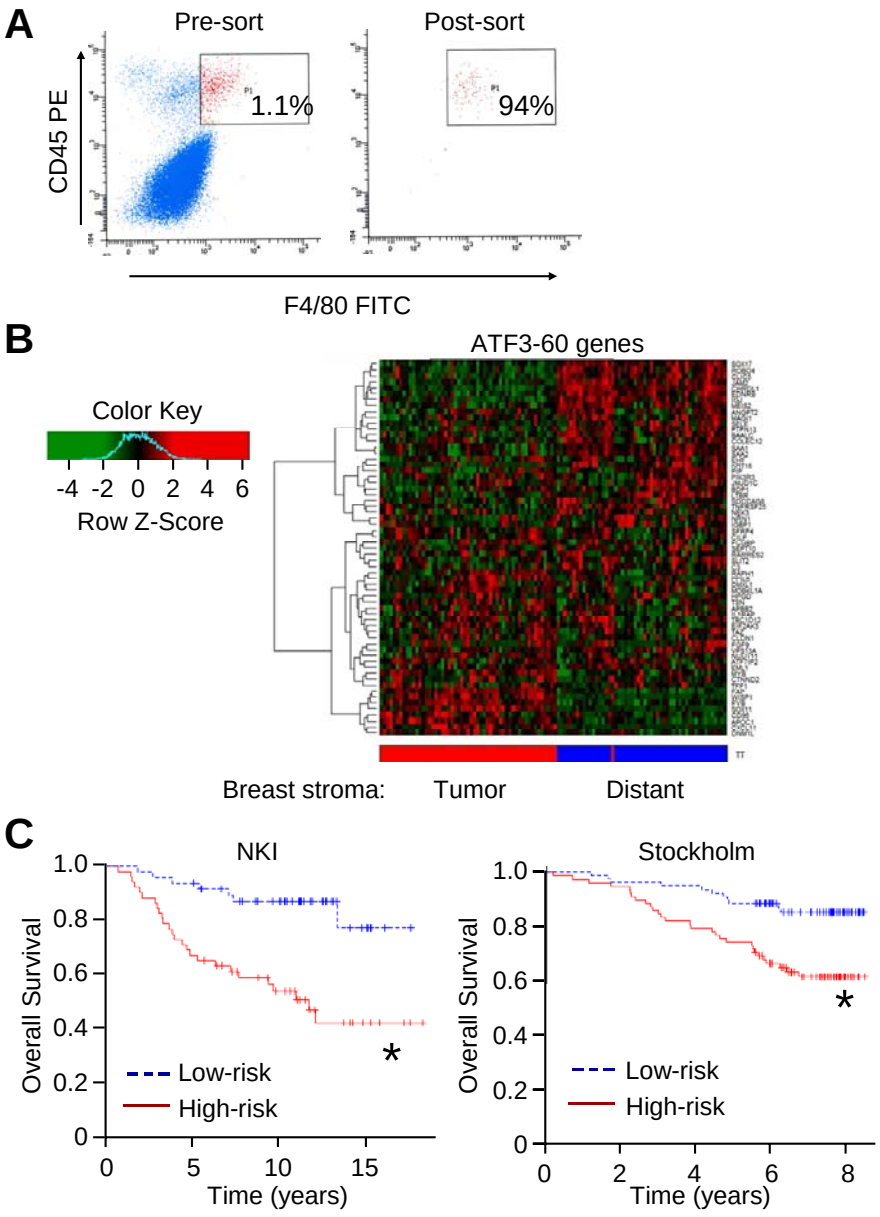

Figure S7

Analyses of FACS-isolated TAMs from *Atf3*$^{+/+}$ and *Atf3*$^{-/-}$ tumor-bearing mice. **(A)** TAMs were isolated from the WT (*Atf3*$^{+/+}$) or KO (*Atf3*$^{-/-}$) 1º tumors using FACS for CD45 and F4/80 double-positive cells. A representative flow image showed enrichment of TAMs from ~1% pre-isolation to 94% post-isolation. **(B)** Heat map indicates that the ATF3-60 genes are differentially expressed in the stroma of human breast samples based on the McGill stroma microarray dataset (GSE4823, $P < 0.0001$ by Fisher's Exact; $P = 0.009$ by 10,000 random permutations). **(C)** A subset ATF3-60 genes were available in the Netherland Cancer Institute (NKI, 39/60) and Stockholm (55/60) datasets and could segregate the patients in the respective dataset into high- and low-risk groups as shown by Kaplan-Meier curve for survival (*$P < 0.01$ for NKI, left; *$P < 0.02$ for Stockholm, right; logrank test, 1,000 permutations).

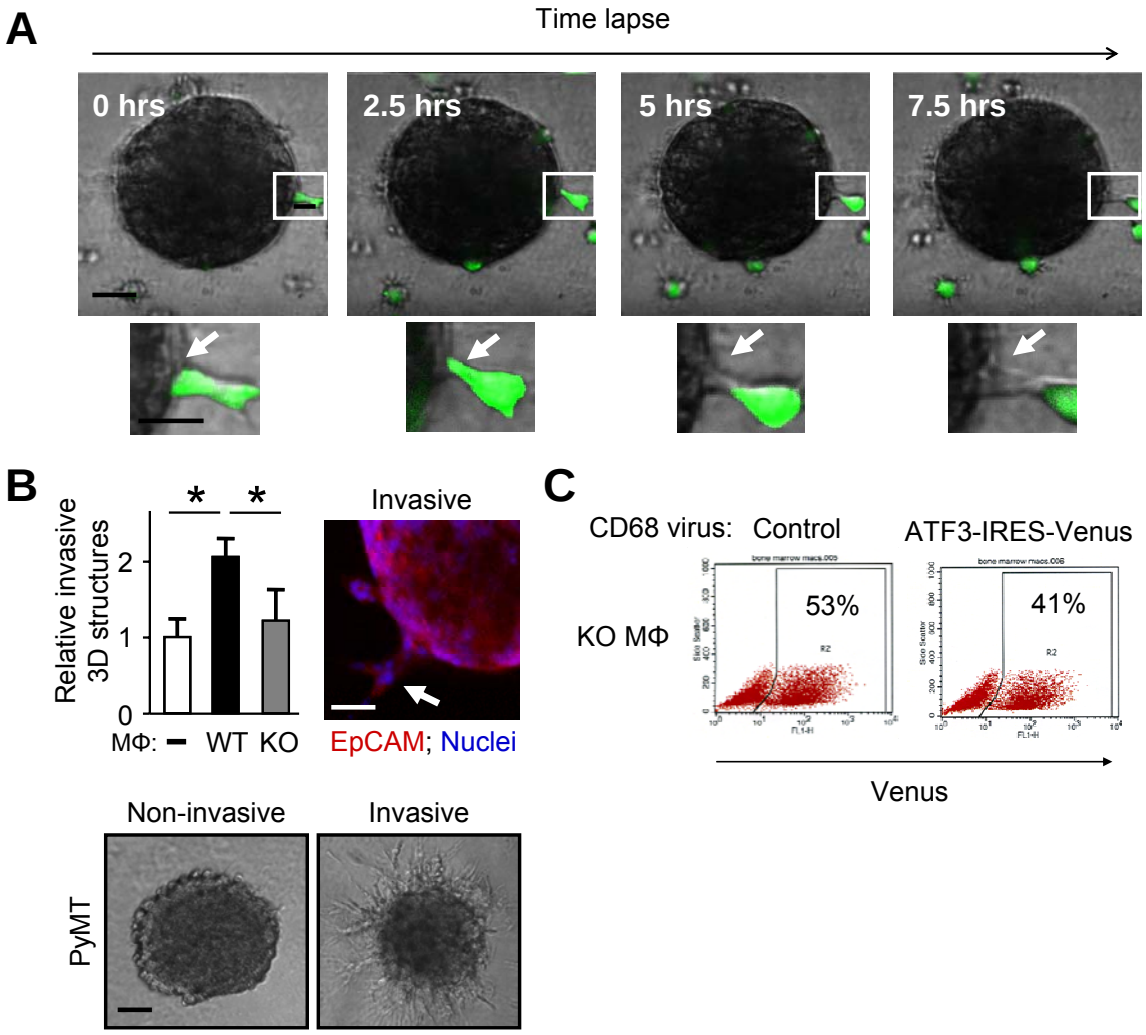

Figure S8

3D co-culture of mammary epithelial cells with bone marrow-derived macrophages (MΦ). **(A)** 3D structures of MCF10A cells were co-cultured with GFP-expressing WT MΦ and examined over a time course by spinning disc confocal microscopy. An interaction between a 3D structure and MΦ is shown (indicated by arrow). Time point 0 is at 19 hours after co-culture. Scale bars = 50μm (low magnification); 25μm (high magnification). **(B)** 3D structures of PyMT cells grown on matrigel were cultured in the absence (-) or presence of MΦ from WT (*Atf3*$^{+/+}$) or KO (*Atf3*$^{-/-}$) mice. Percentage of invasive 3D structures was scored and depicted as in Figure 6A. Immunofluorescent analysis of EpCAM (an epithelial marker, red) and staining of nuclei by Topro-3 (blue) showed cells in the protrusion (upper right). Representative phase contrast images of non-invasive and invasive 3D structures are shown (lower panels). Scale bars = 50μm. **(C)** *Atf3* KO MΦ was transduced with retrovirus expressing Venus (control) or ATF3 plus Venus (ATF3-IRES-Venus) under the control of the CD68 mini-gene cassette. The transduction efficiency was examined by flow cytometry for Venus.

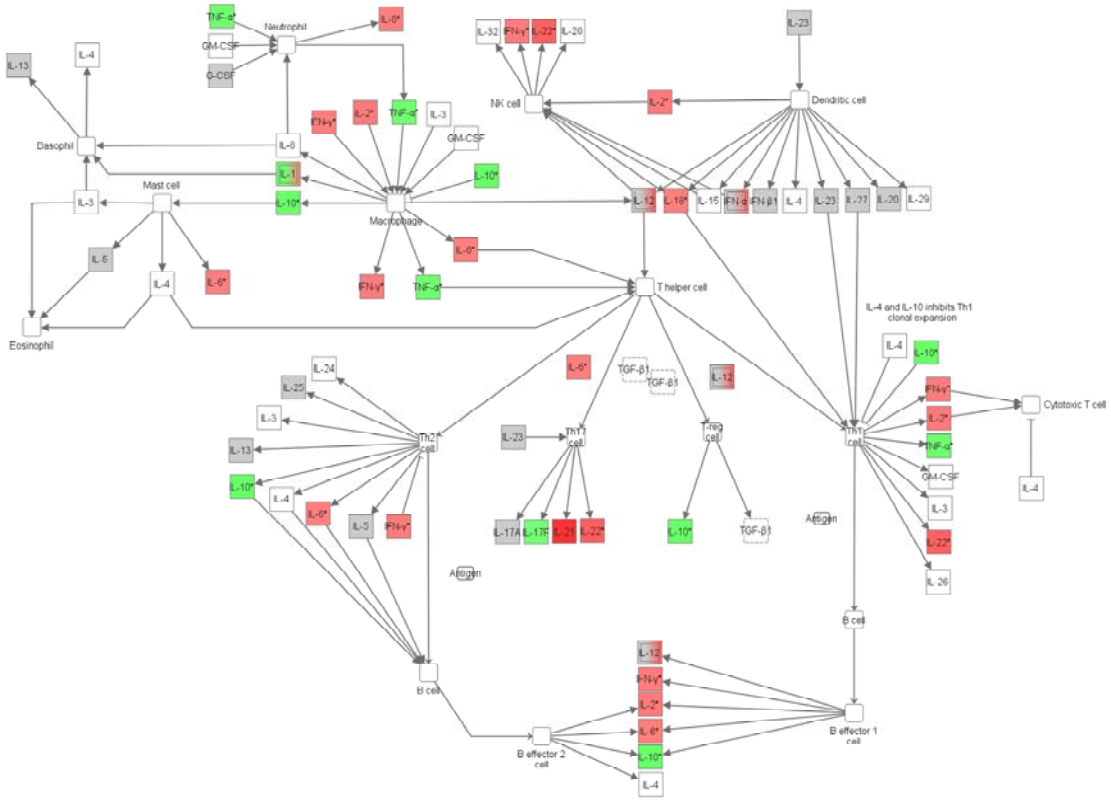

Figure S9

A subset of genes regulated by ATF3 as shown by the Ingenuity Pathway Analyses (IPA). Cytokines in immune cell communication, as depicted by the IPA program, are shown. Green indicates factors that are higher in WT (*Atf3*$^{+/+}$) than KO (*Atf3*$^{-/-}$) TAMs and are thus potential target genes up-regulated (directly or indirectly) by ATF3. Red indicates potential targets down-regulated by ATF3.

SUPPLEMENTAL METHODS

Tumor models and analyses. For the spontaneous metastasis models, 40 μl of a 1:1 mixture containing matrigel (BD Biosciences) and cancer cells (2 x 10^6 PyMT , 2 x 10^5 MVT-1, or 2 x 10^6 Met-1) was injected into the fourth mammary fat pad. Tumor volume was calculated as width^2 x length/2. For Met-1 (a generous gift from Dr. A. Borowsky at University of California, Davis, California) and PyMT cells, primary (1º) tumors were removed when they reached ~1-1.2 cm^3. Mice were euthanized at the indicated time and the lungs inflated with formalin followed by either (a) surface counting of the nodules and measuring by caliper, or (b) analyses of the sections. Briefly, formalin-fixed paraffin embedded lung sections (3 sections per mouse spaced 200 μm apart) were stained with hematoxylin and eosin. The micro-nodules were counted or analyzed by ImageJ for pixel counts (under the green channel for high contrast between nodules and parenchyma). The pixel numbers of the nodules were divided by that of the total lung area, and the average of 3 sections was obtained for each mouse. For lung colonization assay, cancer cells (3 x 10^6 PyMT, 2.5 x 10^6 MVT-1, or 2 x 10^6 Met-1 in 200 μl PBS) were injected via tail vein and the lung analyzed either on the surface (PyMT) or on stained sections (MVT-1 and Met-1). For early time point analysis, turbo GFP (tGFP)-labeled MVT-1 cells were injected by tail vein and lung sections collected at 4, 8, 16, or 24 hours. tGFP-positive cells were stained by immunofluorescence and counted under 200X magnification to obtain the number of cells per 1,000 pixel area of lung section.

Generation of the Atf3$^{f/f}$ mice. Conventional embryonic stem (ES) cell technology was used to generate the *Atf3* flox allele in 129Sv cells by the Transgenic and Embryonic Stem Cell Core (Research Institute at Nationwide Children's Hospital, Columbus, OH). ES cell clones were

screened by Southern blot to identify those containing the targeted allele (*Atf3*^{t}) and the neo cassette was removed by Flip recombinase to generate the flox allele (*Atf3*^{f}). The sequences around the loxP sites were confirmed before blastocyst injection to make the chimera mice. *Atf3*$^{+/f}$ mice were backcrossed into the FVB/N background for 10 generations and the resulting congenic mice were intercrossed to generate the *Atf3*$^{f/f}$ mice.

Plasma analyses by antibody array. Blood from normal or tumor-bearing mice (30 days after orthotopic injection of PyMT cells) was collected by heart puncture and placed into EDTA Microtainer tubes (BD Bioscience) to prevent clotting. After centrifugation, the supernatant (plasma) was pooled from 5 mice per group and analyzed using a mouse L-series biotin label-based antibody array that detects 308 proteins (RayBiotech). Signals for each protein (in duplicate) were obtained by subtracting background signals and normalizing against internal controls.

Generation of the PyMT cancer cell line and general cell culture work. PyMT mammary carcinoma cells (*Atf3*$^{+/+}$, in C57BL/6 background) were isolated from 1º tumors in the MMTV-PyMT transgenic mice at 6 months of age using standard collagenase and sedimentation method (3, 4). The final sedimented material was cultured in growth medium (DMEM/F-12, 10% FBS) for 3 days to allow the epithelial cells to migrate out and adhere to the plates. Differential trypsinization was used to remove contaminating cell types and a morphologically homogeneous culture was obtained after six passages. Flow cytometry analysis showed ~100% EpCAM-positive cells and immunoblot showed PyMT expression. The MVT-1, Met-1, Raw264.7 (Raw), and MCF10A cells were cultured as previously (5-7).

Retroviral production and transduction of cell lines. Stable Raw cells were generated by retroviral transduction according to standard protocols (8) using supernatants from amphotropic Gryphon cells (Allele Biotech) transfected with either pBabe-Puro expressing the puromycin (Puro) resistant gene (vector control) or pBabe-Puro-ATF3. Two days after infection, Raw cells were selected with 2 μg/ml puromycin. tGFP-labeled MVT-1 and Met-1 cells were generated by retroviral transduction using supernatants from Gryphon cells transfected with LZRS-UbC-tGFP-IRES-Puro. Two days after infection, MVT-1 or Met-1 cells were selected with 3.5 μg/ml puromycin and clonal isolates showing strong, homogeneous tGFP expression were obtained.

3D co-culture and trans-endothelial migration assays. 3D co-cultures were established as previously described (1, 9). Briefly, 8-well chamber slides were coated with growth factor-reduced matrigel (BD Bioscience) and incubated at 37ºC until solidified. Cancer cells (10^3 MCF10A or PyMT) were seeded on these slides, cultured for 12-14 days to establish 3D structures, and then overlaid with 5 x 10^3 bone marrow derived-macrophages (see below) in medium with 2% matrigel and IL4 (20 ng/ml; R&D Systems). MMP9 inhibitor I (10 nM, #444278 EMD Biosciences) was added 1 hr prior to the addition of macrophages. Trans-endothelial migration assay was performed as previously described (10). Briefly, 5 x 10^4 human umbilical endothelial cells (HUVECs) (Millipore) were seeded onto transwell inserts (8μm pore size) that had been pre-coated with human fibronectin (50 μg/mL in PBS; Millipore). Two days after seeding, HUVEC monolayers were confirmed by light microscopy. Transwell inserts were then transferred into wells that had either been pre-seeded with bone marrow-derived macrophages or macrophage conditioned medium. tGFP-labeled MVT-1 cells (2 x 10^5) were added on top of the HUVEC monolayer and trans-endothelial migration was assessed 16-20 hrs

later by fluorescent microscopy of the bottom of the transwell insert after removing all remaining cells from the top of the insert.

Bone marrow-derived cells (BMDCs), transduction, and in vitro differentiation. Femurs and tibias from both hind legs of euthanized mice were removed, cleaned, and briefly submerged in 70% ethanol. The ends of each bone were cut off and the marrow flushed with PBS into a tube under sterile condition. The cells were pelleted, washed with PBS, and passed through a 40μm filter to remove particulates or clumps of cells. Red blood cells were lysed in BD Pharm Lyse buffer (BD Bioscience) and the remaining cells washed and resuspended in PBS. These BMDCs were either used immediately or frozen for future use. Retroviral transduction of BMDCs was carried out as previously described (11). Briefly, retroviral supernatant was generated by transfection of Gryphon cells with LZRS-SIN-CD68 vector encoding GFP (control, CD68-GFP), or constitutively active Mmp9 (CD68-Mmp9) (both from Dr. E. Raines at the University of Washington, Seattle, Washington), or ATF3 (CD68-ATF3-IRES-Venus), under the control of the macrophage-selective CD68 mini-gene promoter (11). Because the vector also encodes puromycin resistant gene, the transfected Gryphon cells were treated with puromycin (5 μg/ml) to select retrovirus-producing cells, thus increasing the viral titers in the supernatant. BMDCs were transduced with these retroviral supernatants supplemented with 20% L929 conditioned medium by spin infection: two rounds of centrifugation (2 hrs, 1000 x g, 37ºC) on consecutive days (one round per day). Upon completion of the second round of spin transduction, the cells were induced to differentiate into macrophages or myeloid cells as below. For macrophages, BMDCs were cultured in differentiation medium (DMEM/F-12 supplemented with 10% FBS and 20% conditioned media from L929 cells) for 2 days, the unattached cells harvested and re-

plated in the fresh differentiation medium on non-tissue culture dishes for 7 days with one change of medium. Macrophages were harvested by trypsinization and an aliquot examined by flow cytometry for F4/80 (in general, >99% positive). For $CD11b^+$ myeloid cells, BMDCs were cultured in differentiation medium for 2 days, the unattached cells harvested and analyzed by flow cytometry for CD11b (in general, ~80% positive).

Bone marrow transplantation. Recipient C57BL/6 mice were myeloablated by whole body X-ray irradiation using an RS-2000 device (Rad Source) given in two equal doses (500 Rads each) spaced 3 hours apart and housed under sterile conditions afterwards. Within 5 hours after the second irradiation, the mice were injected with the indicated BMDCs (5×10^6) via tail vein. Thirty days after bone marrow transplant, mice were either injected with the PyMT breast cancer cells via tail vein or euthanized for blood cell analysis by RT-qPCR for *Atf3* to determine transplant efficiency.

Isolation of cells from blood or 1º tumors for RNA analyses. Blood was collected from mice by heart puncture, placed into EDTA Microtainer tubes (BD Bioscience) to prevent clotting, and centrifuged to pellet the cells. Red blood cells were lysed as in BMDCs (above), and the remaining cells washed 2X in PBS and resuspended in TRIzol (Invitrogen) for RNA extraction. 1º tumors were incubated in digest buffer (DMEM/F-12, 3 mg/ml collagenase type I, 150 μg/ml DNase I, Sigma-Aldrich) for 1-1.5 hours at 37°C with gentle shaking. An equal volume of cold DMEM/F-12 + 20% FBS was added to the digest, mixed gently, passed through 100 μm and 40 μm filters, followed by centrifugation at 4°C, washes in cold PBS (2X), and suspension in PBS. Single cell suspensions were pre-incubated with CD16/32 antibody (1 μg/10^6 cells, eBioscience)

to block the Fc receptor and then incubated with antibody bound-magnetic beads (prepared as indicated below) at the following ratio: 50 x 10^6 cells with 500 µl EpCAM beads and 100 x 10^6 cells with 250 µl F4/80 beads. The beads were then washed 5X with bead buffer (PBS, 0.1% BSA, 2 mM EDTA) and immediately resuspended in TRIzol (Invitrogen) for RNA extraction. To prepare the beads, sheep anti-rat magnetic Dynal beads (Invitrogen) were coated with antibody according to manufacturer's instructions. Briefly, the beads were washed with bead buffer, incubated with either EpCAM antibody (20 µg per 500 µl beads, eBioscience) or F4/80 antibody (10 µg per 250 µl beads, Invitrogen) at 4°C for 45 minutes, and washed 5X with bead buffer.

Cell isolation and flow cytometry. Single cell suspensions from the indicated tissues were prepared as described above (for cell isolation from 1º tumors). 10 ml of cell suspension was overlaid onto 15 ml of Percoll (10 ml Percoll, 1.5 ml 10X PBS, 3.5 ml water; GE Healthcare) and centrifuged at 3,000 RPM (4°C) for 15 minutes. The interphase was removed, pelleted, and washed in PBS. Cells were resuspended in staining buffer (PBS, 1% FBS), followed by blocking of the Fc receptor and staining with the indicated antibodies for 30 minutes on ice in the dark: CD11b-FITC (BD Bioscience), Gr1-PE (BD Bioscience), VEGFr1-APC (R&D Systems), F4/80-FITC (eBioscience), CD45-APC (eBioscience). Cells were pelleted and washed 3X with staining buffer and either analyzed on a BD FACScalibur flow cytometer (BD Bioscience) or sorted on a BD FACS Aria flow cytometer (BD Bioscience).

Immunohistochemistry and immunofluorescent staining. Immunohistochemistry stains were performed on formalin-fixed paraffin embedded tissue sections as detailed previously (12).

Primary antibodies were as follows: F4/80 (1:40; Invitrogen), CSF1R (1:100), CD68 (1:50; Dako), Pan-keratin (1:500; Cell Signaling), CD45 (1:100; Invitrogen), Ly6G (1:100; BD Pharmingen), and ATF3 (for mouse tissues: 1:200; Santa Cruz Biotechnology; for human tissues: 1:150; Atlas). For immunofluorescence, slides were prepared as for immunohistochemistry. After incubation with the primary antibody and subsequently with the ImmPRESS Polymer Detection Kit, the fluorescent signal was generated and amplified with the Tyramide Signal Amplification Kit (TSA; Perkin Elmer) according to the manufacturer's instructions. Slides were counterstained with Topro-3 (Molecular Probes) and imaged using a Leica TCS SL Confocal Microscope (Leica Microsystems). To quantify *ATF3*-expressing CD68-positive cells, patient samples were stained by co-immunofluorescence. The number of fields analyzed for each patient varied due to the differences in the abundance of $CD68^+$ cells in the samples. Only consistent scores by two investigators examining the slides side-by-side were recorded. The optimal antigen retrieval buffers (using the steamer method) for ATF3 and CSF1R antibodies are different: citrate buffer (pH 6) for ATF3 and Tris-EDTA buffer (pH 9) for CSF1R. For co-immunofluorescence, the condition for ATF3 was used, compromising the images for CSF1R. Although it is possible to find fields with reasonable images (such as Figure 1G), the quality is not uniform throughout the slides, preventing the quantification of the co-immunofluorescent data with a high degree of confidence. An estimation of *ATF3*-expressing CSF1R cells was achieved by detecting ATF3 and CSF1R separately on immediately adjacent serial sections under the most optimal condition for each antibody. The images were scanned using ScanScope FL (Aperio), followed by overlay in silico. Identifiable landmark features based on nuclear stain (Topro-3) were used to facilitate the overlay. Only consistent scores by two investigators were recorded. We note that the analysis is not meant to provide a definitive

percentage of CSF1R-positive cells that express *ATF3*, because the reliance on identifiable features for overlay limits the fields we analyzed and may skew the number. However, our result clearly showed that only a portion of the CSF1R-positive cells express *ATF3*.

RNA extraction, RT-qPCR, chromatin immunoprecipitation, and zymogram. Total RNA was prepared using TRIzol (Invitrogen) according to the manufacturer instructions. Other procedures were performed as previously (13-15).

Bioinformatics analyses of cRNA array data. Microarray of mouse TAMs was performed by the Biomedical Genomics Core of the Research Institute at Nationwide Children's Hospital, Columbus, Ohio. Microarray data from mouse TAMs were analyzed using a 1.8 fold-change cutoff, resulting in 478 differentially expressed unique genes. These genes were queried against a published human breast stroma microarray dataset (GSE4823). Of the 478 mouse genes, 282 genes were represented on the human array platform (Custom Human Agilent Chip) and a heat map was generated for these 282 genes. To achieve better resolution on the heat map and to identify only those genes with highly variable expression across all samples, we used a variance cutoff of >0.5 and obtained 117 genes (ATF3-117 genes). When a cutoff of >1 was used, we obtained ATF3-60 genes. Statistical significance was determined by Fisher's Exact Analysis and a permutation test (10,000 random permutations). These ATF3-117 or ATF3-60 genes were then analyzed against the Stockholm and NKI breast cancer datasets (below) by the Survival Risk Group Prediction Tool (BRB-Array Tools). This regression model allows analysis of survival risk for each individual as a function of the logged gene expression values. The subset of genes that correlated with time through a univariate analysis was obtained using a Cox threshold

significance level of 0.05 and evaluated using 10-fold cross-validation. Kaplan-Meier curves were plotted based on the low- and high-risk groups predicted by this method, and the statistical significance for the survival curves was assessed using logrank statistical *P* value by performing 1,000 permutations. All other parameters were set to default values. The Stockholm dataset consists of 159 breast cancer patients (GSE1456, NCBI) and the NKI dataset consists of 295 patients (16, 17).

Analyses of tumor microarray from breast cancer patients. The tumor microarray used in this study was derived from 292 patients with invasive breast ductal carcinomas at the St. Vincent's Hospital, Sydney, Australia as described previously (18-22). Clinicopathological characteristics of the cohorts were detailed before. Briefly, 40% of tumors were >20 mm, 45% grade >2, 43% lymph node positive, 69% ER positive (H score >10), 57% PR positive (H score >10) and 18% HER2 FISH positive (>2.2 ratio of HER2:chr.17 centrosome). The cohort had a median age of 54 years and was treated with endocrine therapy (49%), chemotherapy (38%), or both (24%). Cases were prospectively followed-up for a median of 85 months and all deaths were recorded but only breast cancer-related deaths (18%) were considered for survival analyses. After immunohistochemistry for ATF3, a board certified pathologist (ML) with no access to the information regarding the patient population assessed ATF3 signals in epithelial cells and mononuclear cells (based on morphology) using the Allred system to obtain a composite score reflecting both the percentage of cells stained and the intensity of the stain. Statistical evaluation was performed using Statview 5.0 Software (Abacus Systems). Baseline characteristics of the cohort were defined using simple frequency distributions and cutoff for *ATF3* expression was determined using an optimal cut-point technique as previously (20, 21). A score of >4 was

defined as high. Associations of dichotomized variables were determined using Chi squared analysis. Univariate analyses using the Kaplan-Meier and Cox proportional hazards model were applied to the cohort for established clinicopathological variables with breast cancer-related death as the end-point. Multivariate Cox proportional hazards analyses used "backwards" modeling to generate resolved models predictive of outcome. A P value of < 0.05 was accepted as statistically significant.

Table S1. Primers used in this study

RT-qPCR		
Adam9	Fwd.	5'-AAGATTGCCAGTTCCTTCCA-3'
	Rev.	5'-AACCAAAGATGACCTGACAC-3'
Adam10	Fwd.	5'-CATTGCTGAGTGGATTGTGG-3'
	Rev.	5'-TTAAAGTGCCTGGAAGTGGT-3'
Adam15	Fwd.	5'-CTCCACAGACTTCCTACCAG-3'
	Rev.	5'-GTCCACAAACATATTTCCACAC-3'
Adam17	Fwd.	5'-GTGAGAAACGAGTACAGGAC-3'
	Rev.	5'-GTGATGAAACAGAGACAGGG-3'
Adamts4	Fwd.	5'-AATTCAGGTATGGATACAGCG-3'
	Rev.	5'-CAGGTAGATGCTCTTGAGAC-3'
Arg1	Fwd.	5'-CCAGAAGAATGGAAGAGTCAG-3'
	Rev.	5'-GGTACATCTGGGAACTTTCCT-3'
Atf3	Fwd.	5'-GAGATGTCAGTCACCAAGTC-3'
	Rev.	5'-CAGTTTCTCTGACTCTTTCTGC-3'
cMyc	Fwd.	5'-CTCAGTGGTCTTTCCCTACC-3'
	Rev.	5'-CTTCTTGCTCTTCTTCAGAGTC-3'
Epcam	Fwd.	5'-TCCCTGTTCCATTCTTCTAAGAG-3'
	Rev.	5'-CCATCTCCTTTATCTCAGCCT-3'
F4/80	Fwd.	5'-ATCTTGGTTATGCTTCCTTCTG-3'
	Rev.	5'-CTTTGCTTTCGATGTCTAGG-3'
Il6	Fwd.	5'-TCTGCAAGAGACTTCCATCC-3'
	Rev.	5'-GAATTGCCATTGCACAACTC-3'
Il12	Fwd.	5'-GGACATCATCAAACCAGACC-3'
	Rev.	5'-GAATTGTAATAGCGATCCTGAG-3'
Mmp2	Fwd.	5'-GTTCTGGAGATACAATGAAGTG-3'
	Rev.	5'-CAGTCTGATTTGATGCTTCC-3'
Mmp3	Fwd.	5'-TTGAAGCATTTGGGTTTCTC-3'
	Rev.	5'-CACTTCCTTTCACAAAGACTC-3'
Mmp9	Fwd.	5'-CAGGAGTCTGGATAAGTTGGG-3'
	Rev.	5'-TCAAGTCGAATCTCCAGACAC-3'
Mmp12	Fwd.	5'-ACTACTGGAGGTATGATGTG-3'
	Rev.	5'-CATTCTTCCTAACAACCAAACC-3'
Mmp13	Fwd.	5'-TTTCTTTATGGTCCAGGCGA-3'
	Rev.	5'-CACATGGTTGGGAAGTTCTG-3'
Mmp14	Fwd.	5'-CAAGTGATGGATGGATACCC-3'
	Rev.	5'-GTGCTTATCTCCTTTGAAGAAGAC-3'
Nos2	Fwd.	5'-AACCCAAGGTCTACGTTCAG-3'
	Rev.	5'-GAAATAGTCTTCCACCTGCTC-3'
PyMT	Fwd.	5'-ACATGCCAATGGAGGATCTG-3'
	Rev.	5'-GCAAATCCCGAAGAATCAGAC-3'
Timp1	Fwd.	5'-GATGAGTAATGCGTCCAGGA-3'
	Rev.	5'-CATCATGGTATCTCTGGTGTG-3'

Timp2	Fwd. Rev.	5'-CTCTGTGACTTCATTGTGCC-3' 5'-CCCATTGATGCTCTTCTCTG-3'
Tnfa	Fwd. Rev.	5'-TGAACTTCGGGGTGATCG-3' 5'-GCTACAGGCTTGTCACTC-3'
Tgfb	Fwd. Rev.	5'-TCACCCGCGTGCTAATGGTGG-3' 5'-GGTAACGCCAGGAATTGTTGC-3'
ChIP		
Mmp9	Fwd. Rev.	5'-CTAAACCCTGAGTTCTGTGGTTT-3' 5'-GGCTAACGCTGCCTTTGCAGAGA-3'
PCR Genotyping		
Atf3 Alleles*	Fwd. Rev. #1 Rev. #2	5'-TTCACTGCTAATAGCTCCTG-3' 5'-TTCATAGCTCAGGGAACATCGG-3' 5'-CAACTCCCTCTCCTCAAGTC-3'

* For genotyping the $Atf3^{+}$, $Atf3^{f}$, and $Atf3^{r}$ alleles, the three primers listed are used in a 2:1:1 ratio (Fwd.: Rev. #1: Rev. #2). The size of the amplified product for each of the alleles are 189bp ($Atf3^{+}$), 347bp ($Atf3^{f}$) and 242bp ($Atf3^{r}$) as shown in Figure 4E.

SUPPLEMENTAL REFERENCES

1. DeNardo, D.G., Barreto, J.B., Andreu, P., Vasquez, L., Tawfik, D., Kolhatkar, N., and Coussens, L.M. 2009. CD4(+) T cells regulate pulmonary metastasis of mammary carcinomas by enhancing protumor properties of macrophages. *Cancer Cell* 16:91-102.

2. Leek, R.D., and Harris, A.L. 2002. Tumor-associated macrophages in breast cancer. *J Mammary Gland Biol Neoplasia* 7:177-189.

3. Pullan, S.E., and Streuli, C.H. 1996. The mammary gland epithelial cell. In *Handbooks in practical cell biology: Epithelial cell culture*. A. Harris, editor. Cambridge, Breat Britain: University Press. 97-121.

4. Santner, S.J., Dawson, P.J., Tait, L., Soule, H.D., Eliason, J., Mohamed, A.N., Wolman, S.R., Heppner, G.H., and Miller, F.R. 2001. Malignant MCF10CA1 cell lines derived from premalignant human breast epithelial MCF10AT cells. *Breast Cancer Res Treat* 65:101-110.

5. Raschke, W.C., Baird, S., Ralph, P., and Nakoinz, I. 1978. Functional macrophage cell lines transformed by Abelson leukemia virus. *Cell* 15:261-267.

6. Pei, X.F., Noble, M.S., Davoli, M.A., Rosfjord, E., Tilli, M.T., Furth, P.A., Russell, R., Johnson, M.D., and Dickson, R.B. 2004. Explant-cell culture of primary mammary tumors from MMTV-c-Myc transgenic mice. *In Vitro Cell Dev Biol Anim* 40:14-21.

7. Soule, H.D., Maloney, T.M., Wolman, S.R., Peterson, W.D., Jr., Brenz, R., McGrath, C.M., Russo, J., Pauley, R.J., Jones, R.F., and Brooks, S.C. 1990. Isolation and characterization of a spontaneously immortalized human breast epithelial cell line, MCF-10. *Cancer Res* 50:6075-6086.

8. Pear, W., Scott, M., and Nolan, G.P. 1997. Generation of high titer, helper-free retroviruses by transient transfection. In *Methods in molecular medicine: Gene therapy protocols*. P. Robbins, editor. Towowa, NJ: Humana Press. 41-57.

9. Debnath, J., Muthuswamy, S.K., and Brugge, J.S. 2003. Morphogenesis and oncogenesis of MCF-10A mammary epithelial acini grown in three-dimensional basement membrane cultures. *Methods* 30:256-268.

10. Ma, C., and Wang, X.F. 2008. In vitro assays for the extracellular matrix protein-regulated extravasation process. *CSH Protoc* doi: 10.1101/pdb.prot5034.

11. Gough, P.J., and Raines, E.W. 2003. Gene therapy of apolipoprotein E-deficient mice using a novel macrophage-specific retroviral vector. *Blood* 101:485-491.

12. Hai, T., Jalgaonkar, S., Wolford, C.C., and Yin, X. 2011. Immunohistochemical detection of Activating Transcription Factor 3, a hub of the cellular adaptive-response network. In *Meth. Enzy.* M.P. Conn, editor. Burlington: Elsevier Inc. Academic Press. 175-194.

13. Lu, D., Wolfgang, C.D., and Hai, T. 2006. Activating transcription factor 3, a stress-inducible gene, suppresses Ras-stimulated tumorigenesis. *J Biol Chem* 281:10473-10481.

14. Yin, X., DeWille, J., and Hai, T. 2008. A potential dichotomous role of ATF3, an adaptive-response gene, in cancer development. *Oncogene* 27:2118-2127.

15. Herron, G.S., Banda, M.J., Clark, E.J., Gavrilovic, J., and Werb, Z. 1986. Secretion of metalloproteinases by stimulated capillary endothelial cells. II. Expression of collagenase and stromelysin activities is regulated by endogenous inhibitors. *J Biol Chem* 261:2814-2818.

16. van 't Veer, L.J., Dai, H., van de Vijver, M.J., He, Y.D., Hart, A.A., Mao, M., Peterse, H.L., van der Kooy, K., Marton, M.J., Witteveen, A.T., et al. 2002. Gene expression profiling predicts clinical outcome of breast cancer. *Nature* 415:530-536.

17. van de Vijver, M.J., He, Y.D., van't Veer, L.J., Dai, H., Hart, A.A., Voskuil, D.W., Schreiber, G.J., Peterse, J.L., Roberts, C., Marton, M.J., et al. 2002. A gene-expression signature as a predictor of survival in breast cancer. *N Engl J Med* 347:1999-2009.

18. Lopez-Knowles, E., O'Toole, S.A., McNeil, C.M., Millar, E.K.A., Qiu, M.R., Crea, P., Daly, R.J., Musgrove, E.A., and Sutherland, R.L. 2009. PI3K pathway activation in breast cancer is associated with the basal-like phenotypes and cancer-specific mortality. *Int J Cancer* 126:1121-1131.

19. Millar, E.K.A., Anderson, L.R., McNeil, C.M., O'Toole, S.A., Pinese, M., Crea, P., Morey, A.L., Biankin, A.F., Henshall, S.M., Musgrove, E.A., et al. 2009. BAG-1 predicts patient outcome and tamoxifen responsiveness in ER-positive invasive ductal carcinoma of the breast. *Brit J Cancer* 100:123-133.

20. O'Toole, S.A., Machalek, D.A., Shearer, R.F., Millar, E.K., Nair, R., Schofield, P., McLeod, D., Cooper, C.L., McNeil, C.M., McFarland, A., et al. 2011. Hedgehog overexpression is associated with stromal interactions and predicts for poor outcome in breast cancer. *Cancer Res* 71:4002-4014.

21. Lopez-Knowles, E., Zardawi, S.J., McNeil, C.M., Millar, E.K., Crea, P., Musgrove, E.A., Sutherland, R.L., and O'Toole, S.A. 2010. Cytoplasmic localization of beta-catenin is a marker of poor outcome in breast cancer patients. *Cancer Epidemiol Biomarkers Prev* 19:301-309.

22. Zardawi, S.J., Zardawi, I., McNeil, C.M., Millar, E.K., McLeod, D., Morey, A.L., Crea, P., Murphy, N.C., Pinese, M., Lopez-Knowles, E., et al. 2010. High Notch1 protein expression is an early event in breast cancer development and is associated with the HER-2 molecular subtype. *Histopathology* 56:286-296.